Journal of Power Sources 244 (2013) 129–135

Contents lists available at SciVerse ScienceDirect

Journal of Power Sources

journal homepage: www.elsevier.com/locate/jpowsour

Preparation and electrochemical properties of glass-modified $LiCoO_2$ cathode powders

Seung Ho Choi, Jung Hyun Kim, You Na Ko, Kwang Min Yang, Yun Chan Kang*

Department of Chemical Engineering, Konkuk University, 1 Hwayang-dong, Gwangjin-gu, Seoul 143-701, Republic of Korea

HIGHLIGHTS

- Lithium boron oxide glass-modified $LiCoO_2$ nanopowders are prepared by flame spray pyrolysis.
- The glass-modified powders have a mean size of 120 nm and good electrochemical properties.
- The capacity retention of the 5 wt% glass-modified $LiCoO_2$ powders is 98% by the 50th cycle.

GRAPHICAL ABSTRACT

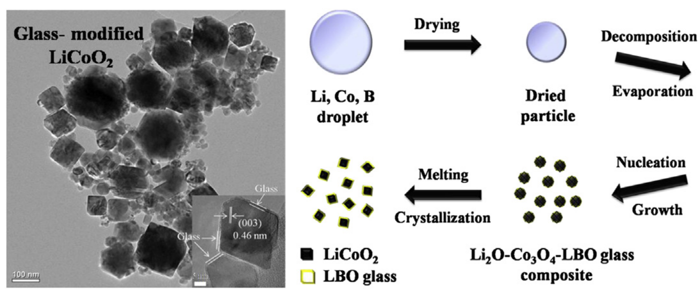

ARTICLE INFO

Article history:
Received 15 October 2012
Received in revised form
6 March 2013
Accepted 8 March 2013
Available online 19 March 2013

Keywords:
Nanoparticles
Flame spray pyrolysis
Lithium cobaltate
Glass material

ABSTRACT

Pure $LiCoO_2$ nanopowders and those coated with lithium boron oxide (LBO) glass are prepared directly using high-temperature flame spray pyrolysis. Prior to post-treatment, the $LiCoO_2$ powders with nanometer-size particles have low discharge capacities and poor cycle properties, irrespective of the amount of glass material. Post-treatment at 500 °C does not improve these properties significantly; however, the LBO glass-modified $LiCoO_2$ powders post-treated at 600 and 700 °C demonstrates good cycle performance. The discharge capacity of the 5 wt% glass-modified $LiCoO_2$ powders post-treated at 600 °C with a mean particle size of 120 nm, decreases from 122 to 109 mAh g^{-1} after 50 cycles, with a capacity retention of 89%. The capacity retentions of the pure and 2, 5, and 10 wt% glass-modified $LiCoO_2$ powders post-treated at 700 °C are 86, 96, 98, and 98% after 50 cycles, respectively.

1. Introduction

Lithium ion batteries that utilize $LiCoO_2$ as the cathode material are widely used [1–3]. However, there is a great deal of ongoing research with the aim of improving the performance of this material [4–8]. $LiCoO_2$ in the form of a nanopowder has been investigated because of the potential that its large surface area and enhanced Li intercalation efficiency have for achieving a high power and high energy density [9–13]. Various types of chemical processes, such as sol–gel, hard templating, and hydrothermal, have been applied to prepare $LiCoO_2$ nanopowders with good morphological and electrochemical properties [9–13]. In conventional processes, $LiCoO_2$ nanopowders are prepared by high-temperature post-treatment of the intermediate product obtained from the precursor salts of Li and Co components. However, hard aggregation of the $LiCoO_2$ nanopowders was found to occur during the decomposition and solid-state reaction of Li and Co components [13–15]. Therefore, non-aggregated $LiCoO_2$ nanopowders with high crystallinity could not be successfully produced using conventional solution processes.

Flame spray pyrolysis is a technique widely used to synthesize a number of functional powders over sizes ranging from nanometers to micrometers [16–23]. Cathode nanopowders with a pure single

* Corresponding author. Tel.: +82 2 2049 6010; fax: +82 2 458 3504.
E-mail address: yckang@konkuk.ac.kr (Y.C. Kang).

0378-7753/$ – see front matter © 2013 Elsevier B.V. All rights reserved.
http://dx.doi.org/10.1016/j.jpowsour.2013.03.028

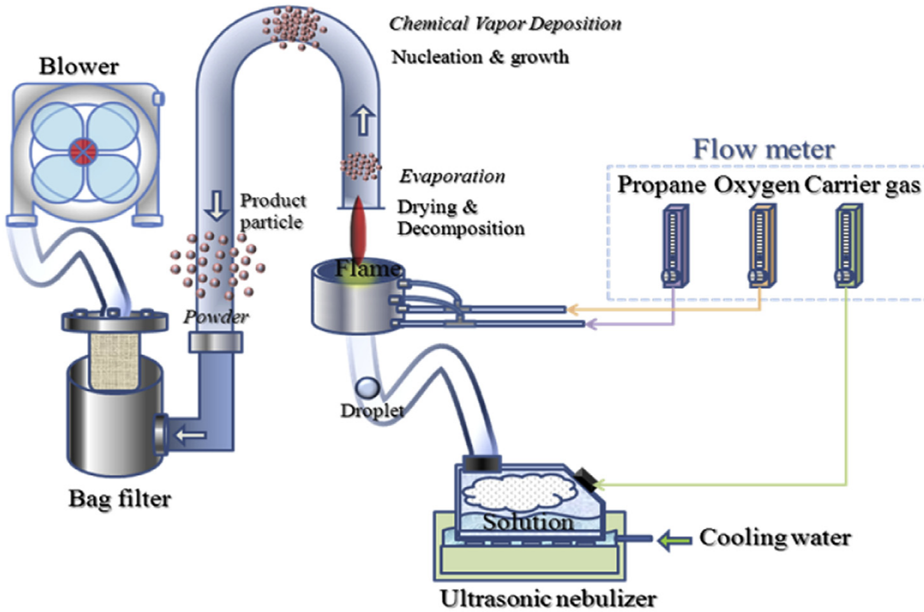

Fig. 1. Schematic diagram of the flame spray pyrolysis for glass-modified $LiCoO_2$ nanopowders.

crystalline structure have been prepared directly by high-temperature flame spray pyrolysis without post-treatment [19–23]. However, the electrochemical properties of these nanopowders were improved by treatment at high temperatures [23]. These single crystalline cathode nanopowders had high thermal stability during the post-treatment process, meaning that particle growth and aggregation between the particles was minimized.

Cathode nanopowders suffer from high fading rates because of their large electrode/electrolyte interface areas and poor crystallinity [24–26]. To improve the electrochemical properties of $LiCoO_2$ nanopowders, surface modification by stable oxide materials has proven to be effective [27–32]. Lithium boron oxide (LBO) glass has previously been used as a coating material because of its high Li ion conductivity, good wetting properties, and relatively low viscosity [31–35]. In this study, pure and LBO glass-coated $LiCoO_2$ nanopowders were prepared directly by high-temperature flame spray pyrolysis. The physical and electrochemical properties of the synthesized nanopowders post-treated at various temperatures were investigated.

2. Experimental

The schematic diagram for the flame spray pyrolysis system used in this study is shown in Fig. 1. The flame spray pyrolysis system has a droplet generator, flame nozzle, powder collector, and blower. A 1.7 MHz ultrasonic spray generator with six resonators was used to generate droplets, which were then carried into the high-temperature diffusion flame by O_2 (carrier gas). Droplets or powders evaporated, decomposed, and melted inside the diffusion flame. Propane (fuel) and O_2 (oxidizer) were used to produce the diffusion flame. The flame nozzle consisted of five concentric pipes. Droplets generated from the precursor solution were supplied to the diffusion flame through the central pipe by the carrier gas, with an appropriately varied flow rate. The flow rate of the fuel gas was fixed at 5 L min^{-1}, and the flow rates of the oxidizer and carrier gases were fixed at 40 L min^{-1} and 10 L min^{-1}, respectively.

An aqueous spray solution was prepared by dissolving lithium nitrate ($LiNO_3$, Junsei) and cobalt nitrate hexahydrate [$Co(NO_3)_2\cdot 6H_2O$, Aldrich] in distilled water. The total concentration of the solution was 1.5 M. The amount of Li added to the spray solution was in excess of 20 wt% of the stoichiometric amount, to facilitate the formation of $LiCoO_2$ powders. For the $Li_2O-2B_2O_3$ glass modifier, $LiNO_3$ and boric acid (H_3BO_3, Aldrich) were added into the above Li and Co spray solution. The amount of LBO glass modifier was varied from 2 to 10 wt% of the $LiCoO_2$ powders. The precursor particles obtained by flame spray pyrolysis were post-treated at temperatures of 500, 600, and 700 °C for 3 h in an air atmosphere.

The crystal structures of the prepared cathode powders were investigated using X-ray diffractometry (XRD, X'pert PRO MPD) with Cu Kα radiation (λ = 1.5418 Å). Morphological characteristics were investigated using scanning electron microscopy (SEM, JEOL JSM-6060) and high-resolution transmission electron microscopy (TEM, JEOL-2100F) at 200 kV. The XPS spectra of the pure and 5 wt% glass-modified $LiCoO_2$ powders were investigated using X-ray photoelectron spectroscopy (XPS, ESCALAB-210) with Al Kα radiation (1486.6 eV). The binding energy was calibrated with reference to the C 1s level of carbon (284.5 eV). The elemental composition of

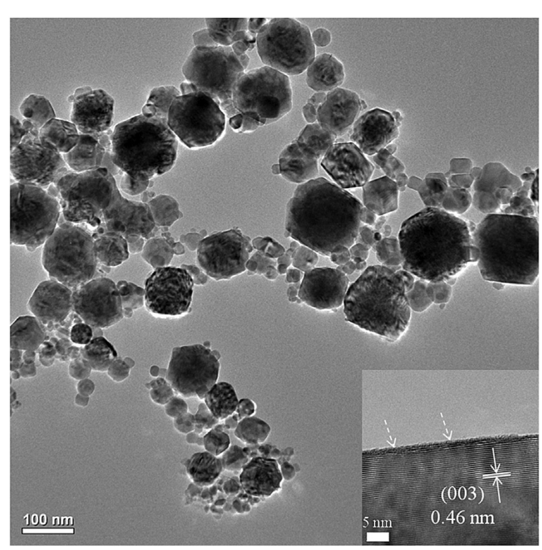

Fig. 2. TEM image of the pure $LiCoO_2$ powders prepared directly by flame spray pyrolysis.

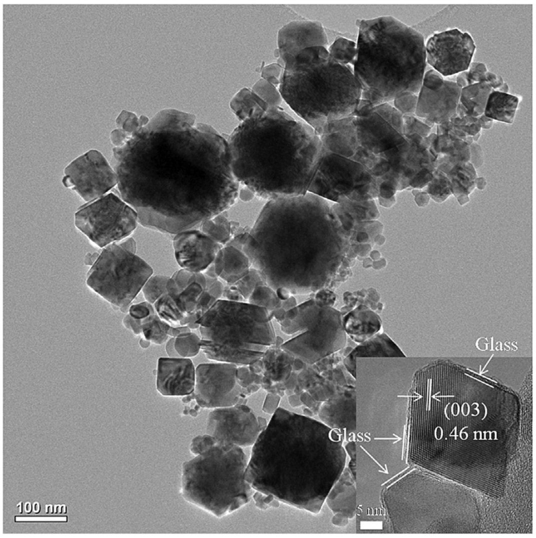

Fig. 3. TEM image of the LBO-glass modified $LiCoO_2$ powders prepared directly by flame spray pyrolysis.

the 5 wt% LBO glass-modified $LiCoO_2$ powders was investigated using an inductively coupled plasma-optical emission spectrometer (ICP-OES, Thermo elemental, ICAP 6000).

The capacities and cycle properties of the powders were determined using a 2032-type coin cell. The cathode electrode was prepared from a mixture containing 15 mg $LiCoO_2$ and 9 mg TAB (TAB is a mixture of 7.2 mg teflonized acetylene black and 1.8 mg of a binder). Li metal and microporous polypropylene film were used as the anode and separator, respectively. The electrolyte was 1 M $LiPF_6$ in a 1:1 mixture (v/v) of ethylene carbonate/dimethyl carbonate (EC/DMC). The charge/discharge characteristics of the samples were determined through cycling in the 3.2–4.2 V potential range at a constant current density of 0.5 C (70 mA g^{-1}). Cyclic voltammetry measurements were carried out at a scan rate of 0.07 mV s^{-1}.

3. Results and discussion

The morphologies of the pure and LBO glass-modified $LiCoO_2$ powders prepared by flame spray pyrolysis are shown in Figs. 2 and 3. The sizes of the prepared powders were on the scale of nanometers and no aggregation was apparent, irrespective of the amount of glass modifier. Complete evaporation of Li, Co, and B components occurred inside the high-temperature diffusion flame,

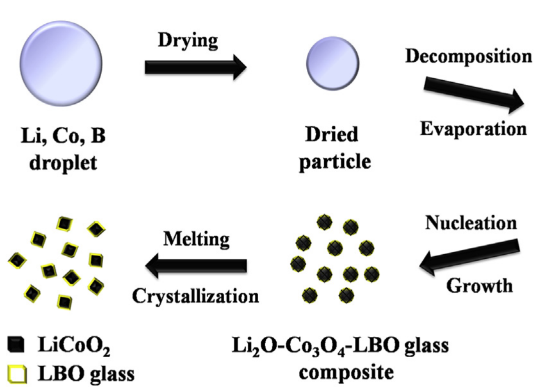

Fig. 4. Schematic diagram of formation mechanism of glass-modified $LiCoO_2$ powders in the flame spray pyrolysis.

forming the nanoscale cathode powders from the vapors by nucleation and growth processes. No micron or submicron-sized particles, obtained because of incomplete evaporation of the intermediate powders, can be observed in the SEM images. The mean sizes of the pure and LBO glass-modified $LiCoO_2$ powders measured from the low-resolution TEM images were 42 and 54 nm, respectively, and both had a polyhedral structure with clear crystal fringes. The high-resolution TEM images exhibit clear lattice fringes with a separation of 0.46 nm and a polycrystalline structure, irrespective of the amount of glass modifier. This value corresponds to the (003) plane of the α-$NaFeO_2$ layered structure type of $LiCoO_2$ [13]. The LBO-modified $LiCoO_2$ particles were coated with a glass layer that was approximately 1 nm thick (Fig. 3b). The mechanism

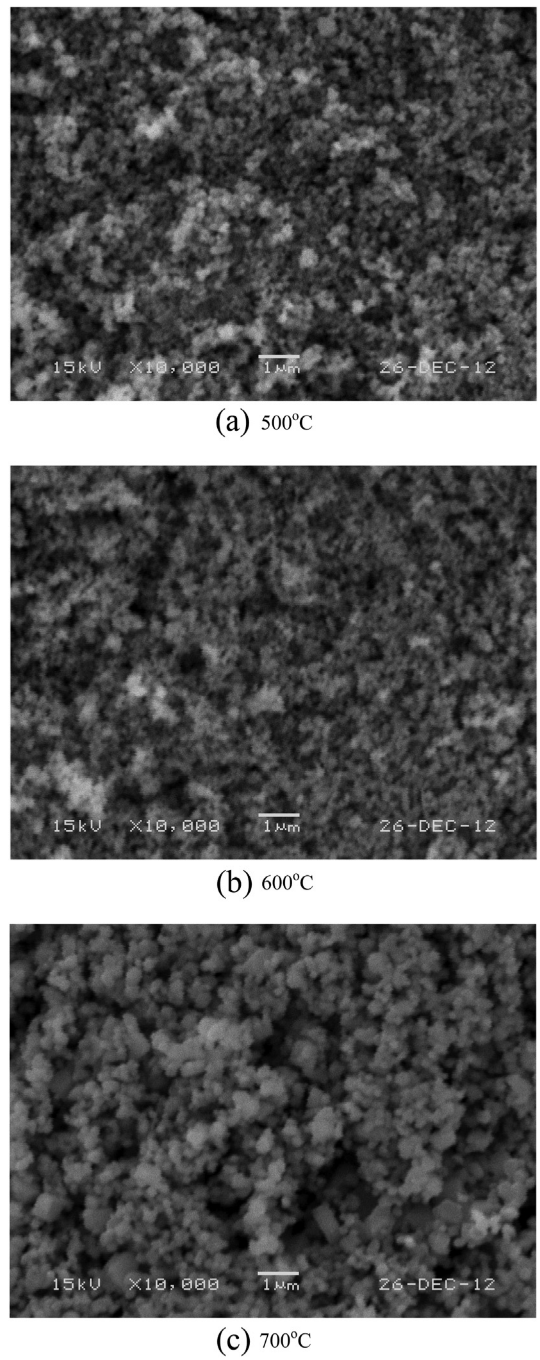

Fig. 5. SEM images of the pure $LiCoO_2$ powders post-treated at various temperatures.

of formation of the LBO glass-modified $LiCoO_2$ powders is described in Fig. 4. Collisions of vapor molecules inside the diffusion flame formed composite oxide powders of Li, Co, and B components, and $LiCoO_2$ crystals grew by the reaction of Li_2O and Co_3O_4 inside the nanometer-sized powder particles. The B component had low solubility in the $LiCoO_2$ crystals. LBO glass material with an amorphous structure has been easily formed from the B and Li components at high temperatures [36]. Therefore, LBO glass material formed from B and Li components migrated to the outside edges of the nanometer-sized particles during the crystallization process. No pores were observed within the polycrystalline structure of the particles on the high-resolution TEM images. The images show that the small amount of glass material did not affect the morphologies of the $LiCoO_2$ powders.

The initial charge/discharge capacities and cycle properties of the pure and LBO glass-modified $LiCoO_2$ cathode powders prepared directly by flame spray pyrolysis were investigated. The initial charge and discharge capacities of the pure $LiCoO_2$ powders were 97 and 79 mAh g^{-1}, respectively, and those of the 10 wt% LBO glass-modified $LiCoO_2$ powders were 83 and 74 mAh g^{-1}, respectively. The discharge capacities of the pure and LBO glass-modified $LiCoO_2$ cathode powders were reduced to 62 and 66 mAh g^{-1}, respectively, after 10 cycles. The $LiCoO_2$ powders were seen to have poor crystallinities because of the short residence time of the powders inside the high-temperature diffusion flame. The amorphous surface layer of the pure $LiCoO_2$ particles shown by an arrow in Fig. 2b demonstrates the poor crystallinity of the powders. In order to improve the crystallinities and the electrochemical properties of the $LiCoO_2$ powders, they were post-treated at temperatures between 500 and 700 °C for 3 h. Figs. 5 and 6 show SEM images of the pure and LBO

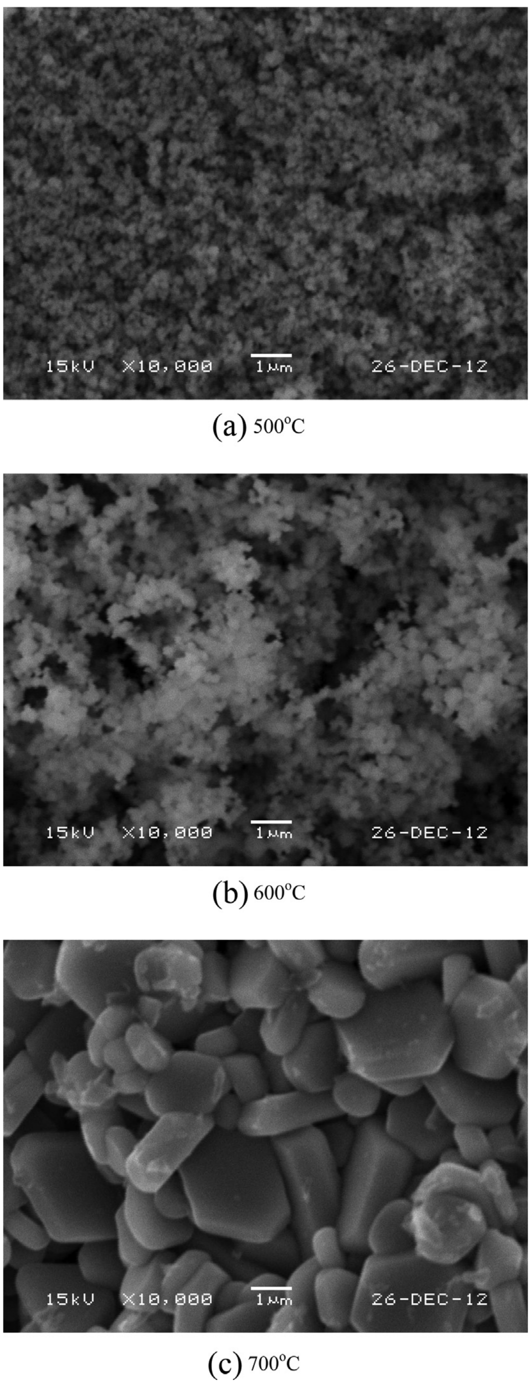

Fig. 6. SEM images of the LBO glass-modified $LiCoO_2$ powders post-treated at various temperatures.

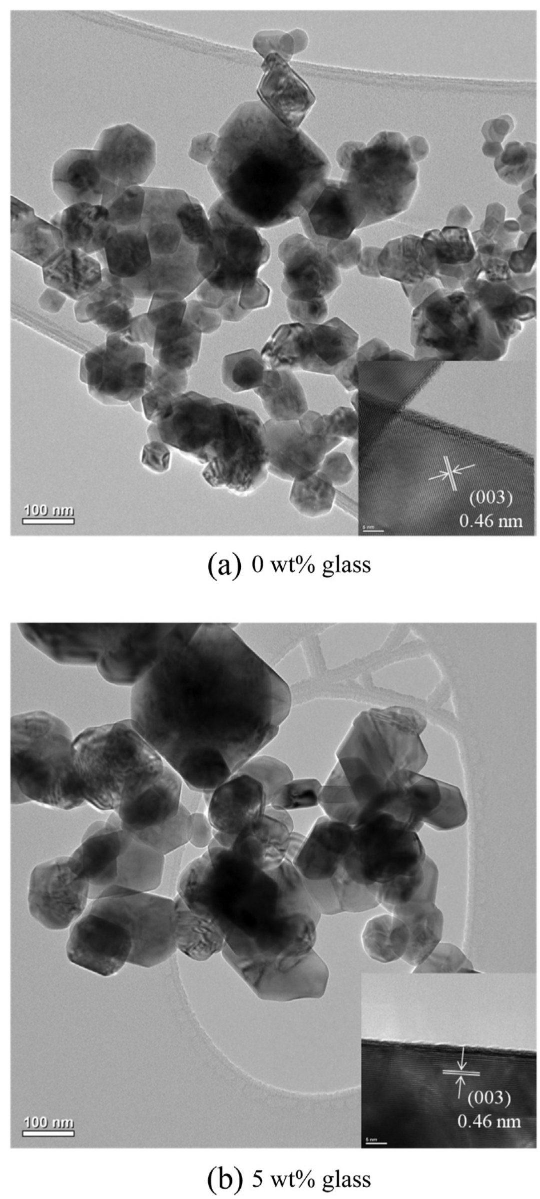

Fig. 7. TEM images of the pure and LBO glass-modified $LiCoO_2$ powders post-treated at 600 °C.

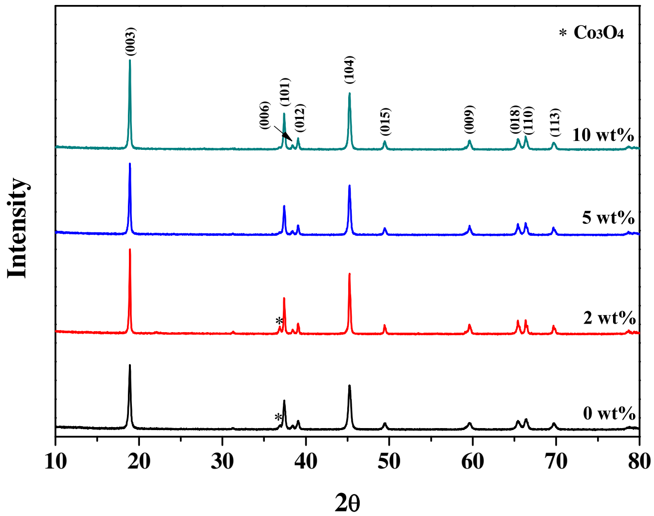

Fig. 8. XRD patterns of the pure and LBO glass-modified $LiCoO_2$ powders post-treated at 600 °C.

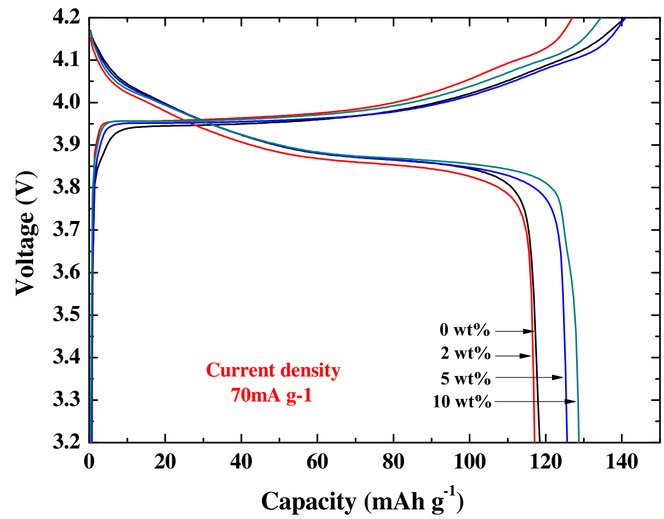

Fig. 9. Initial charge/discharge curves of the pure and LBO glass-modified $LiCoO_2$ powders post-treated at 600 °C.

glass-modified $LiCoO_2$ powders post-treated at various temperatures. The cathode powders treated at temperatures of 500 and 600 °C had fine particle sizes, irrespective of LBO glass material. However, the LBO glass strongly affected the morphologies of the $LiCoO_2$ powders that were treated at 700 °C. These samples had particles on the micron-scale and a well-faceted crystal structure. The melting temperature of the LBO glass material is 580 °C. Therefore, the LBO glass material acted as a sintering agent above this temperature, causing an increase in the mean particle size and improved crystallinity of the $LiCoO_2$ powders. The pure $LiCoO_2$ particles were only several hundred nanometers in dimension, even at a high post-treatment of 700 °C. Fig. 7 shows low and high-resolution TEM images of the pure and 5 wt% glass-modified $LiCoO_2$ powders post-treated at 600 °C. The sizes of the $LiCoO_2$ powders, with and without the glass modification, can be seen to be on the scale of nanometers with well-faceted crystal structures. The mean sizes of the powders with and without 5 wt% glass measured from the TEM images were 92 and 120 nm, respectively. The use of the glass modifier slightly increased the mean size of the $LiCoO_2$ powders at a post-treatment temperature of 600 °C. High-resolution TEM images exhibit clear lattice fringes with a separation of 0.46 nm, irrespective of the amount of glass material. This value corresponds to the (003) plane of the α-$NaFeO_2$ layered structure type of $LiCoO_2$ [13].

Fig. 8 shows XRD patterns of the pure and LBO glass-modified $LiCoO_2$ powders post-treated at 600 °C. The pure and 2 wt% LBO glass-modified $LiCoO_2$ powders had small peaks due to Co_3O_4 impurity. However, the impurity peaks of Co_3O_4 phase were not observed from the XRD patterns of the 5 and 10 wt% LBO glass-modified $LiCoO_2$ powders. The mean crystallite sizes of the pure and LBO glass-modified $LiCoO_2$ powders post-treated at various temperatures calculated from the widths of the (003) peaks using Scherrer's equation are summarized in Table 1. The LBO-glass modified $LiCoO_2$ powders had higher mean crystallite sizes than those of the pure $LiCoO_2$ powders at all post-treatment temperatures. The mean crystallite sizes of the powders increased with increasing temperature for all samples. The lattice parameter ratios (c/a) of the pure and 5 wt% LBO glass-modified $LiCoO_2$ powders were 4.99 and 4.97, respectively. Doping with B, with its small radius, in the $LiCoO_2$ phase decreased the lattice parameter ratio. The composition of 5 wt% LBO glass-modified $LiCoO_2$ powders was $Li_{0.99}B_{0.05}CoO_2$, as determined by ICP analysis. The ratio of Li and Co components of the glass-modified $LiCoO_2$ was similar to that of stoichiometric $LiCoO_2$.

Fig. 9 shows the initial charge/discharge curves of the pure and LBO glass-modified $LiCoO_2$ powders post-treated at 600 °C. The operating cut-off voltages were 3.2 and 4.2 V at a current density of 70 mA g^{-1}. The initial capacities and Coulombic efficiencies of the $LiCoO_2$ powders are summarized in Table 2. The LBO glass-modified $LiCoO_2$ powders with high phase purity and high crystallinity had higher initial charge/discharge capacities and Coulombic efficiencies than those of the pure $LiCoO_2$ powders in Figs. 8 and 9.

Fig. 10 shows the cycle properties of the pure and LBO glass-modified $LiCoO_2$ powders post-treated at various temperatures. The operating cut-off voltages were 3.2 and 4.2 V at a current density of 70 mA g^{-1}. The results of cycle properties of the $LiCoO_2$ powders are summarized in Table 2. The $LiCoO_2$ powders post-treated at a low temperature of 500 °C had poor cycle properties, irrespective of the amount of glass material. However, the LBO glass-modified $LiCoO_2$ powders had better cycle performances than those of the pure $LiCoO_2$ powders at post-treatment temperatures of 600 and 700 °C. The discharge capacity of the pure $LiCoO_2$ powders post-treated at 600 °C decreased from 119 to 85 mAh g^{-1} after 50 cycles, with a capacity retention of 71%, whereas as that of the 5 wt% glass-modified $LiCoO_2$ decreased from 122 to 109 mAh g^{-1}, with a capacity retention of 89%. The capacity retentions of the pure and 2,

Table 1
Lattice parameters and mean crystallite sizes of the pure and glass-modifed $LiCoO_2$ powders post-treated at 600 °C.

	a (Å)	c (Å)	c/a	Crystalline size (nm)
0 wt%	2.816	14.069	4.99	36
2 wt%	2.816	14.034	4.98	56
5 wt%	2.817	14.017	4.97	47
10 wt%	2.816	14.043	4.98	47

Table 2
Cycle properties and Coulombic efficiencies of the pure and glass-modified $LiCoO_2$ powders post-treated at 700 °C.

	0 wt%	2 wt%	5 wt%	10 wt%
1st Cap. (mAh g^{-1})	111	118	126	122
Coulombic Eff. (%)	84	92	90	95
50th Cap. (mAh g^{-1})	95	113	123	119
50th Ret. (%)	86	96	98	98

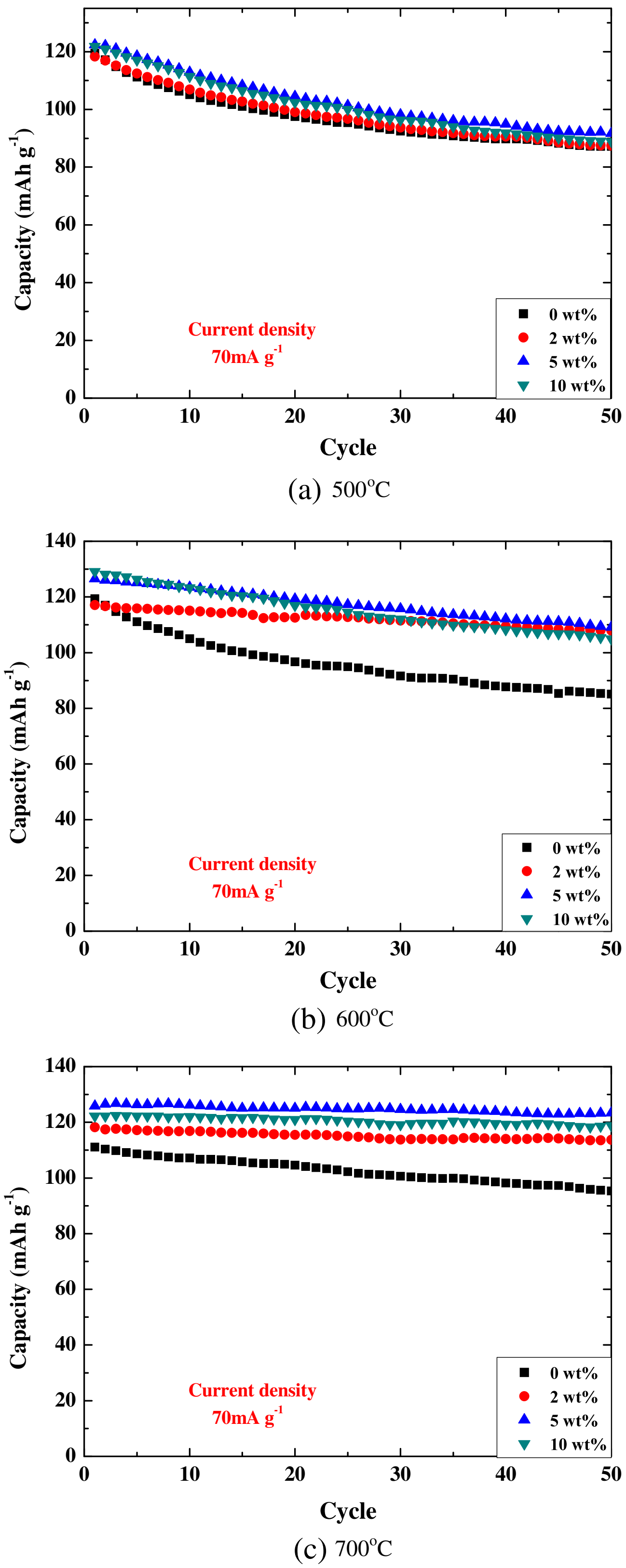

Fig. 10. Cycle properties of the pure and LBO glass-modified $LiCoO_2$ powders post-treated at various temperatures.

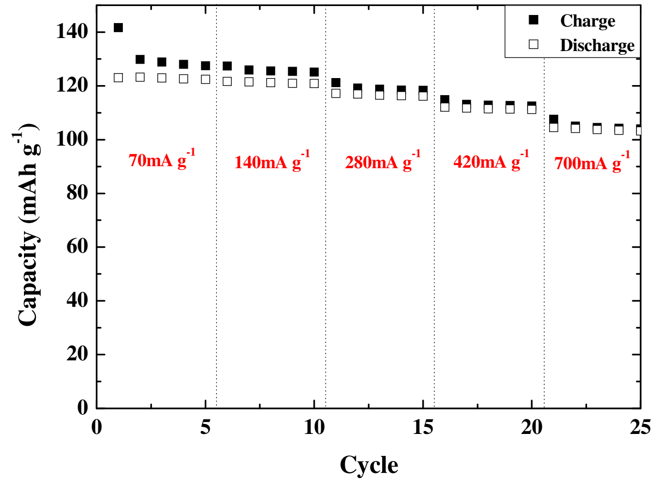

Fig. 11. Rate performances of the 5 wt% LBO glass-modified $LiCoO_2$ powders post-treated at 600 °C.

5, and 10 wt% glass-modified $LiCoO_2$ powders post-treated at 700 °C were 86, 96, 98, and 98% after 50 cycles, respectively. The discharge capacity of the 5 wt% glass-modified $LiCoO_2$ powders post-treated at 700 °C decreased from 126 to 123 mAh g^{-1} after 50 cycles.

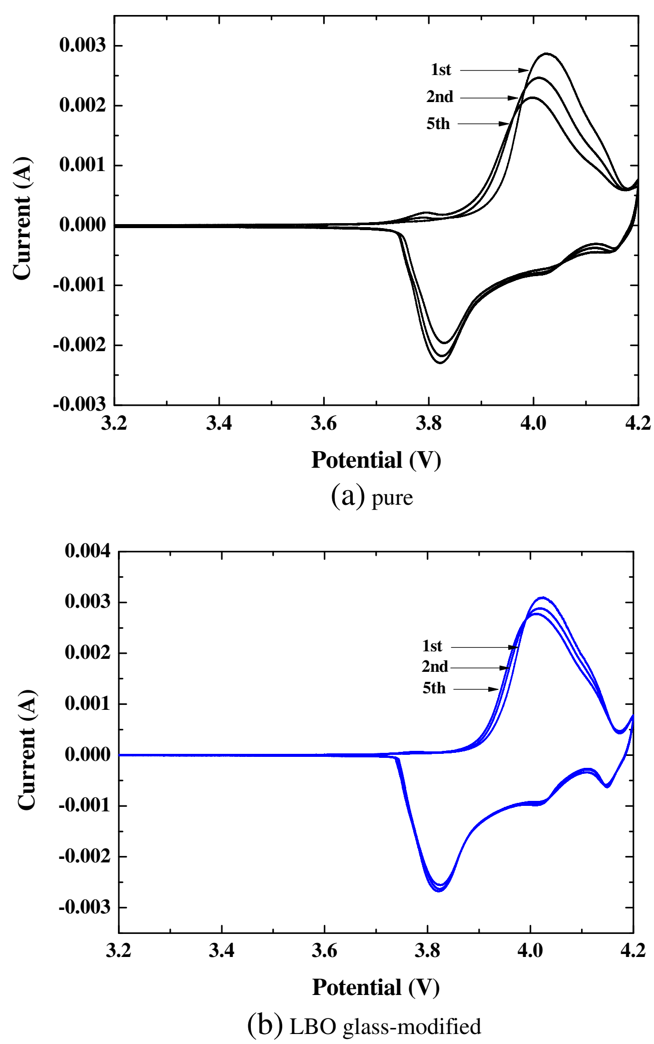

Fig. 12. CV curves of the pure and LBO glass-modified $LiCoO_2$ powders post-treated at 600 °C.

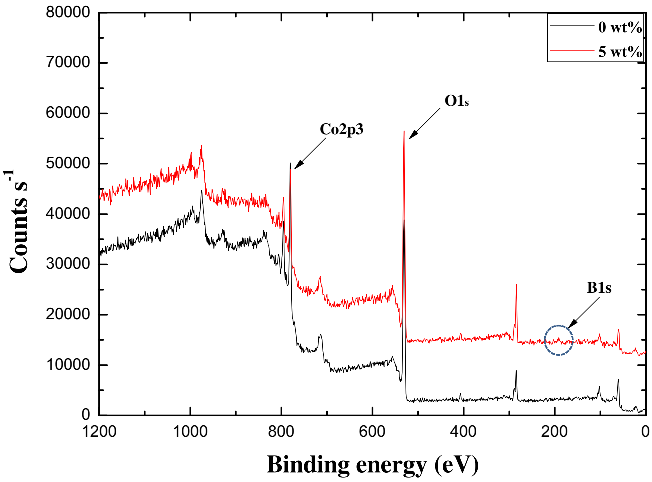

Fig. 13. XPS spectra of the pure and 5 wt% glass-modified $LiCoO_2$ powders post-treated at 600 °C.

The rate performances of the 5 wt% LBO glass-modified $LiCoO_2$ powders post-treated at 600 °C are shown in Fig. 11. The 5 wt% glass-modified $LiCoO_2$ exhibited an initial discharge capacity of 122 mAh g^{-1} at a current density of 70 mA g^{-1} (0.5 C). As the charge/discharge rate increased from 140 to 280, 420 and 700 mA g^{-1}, the discharge capacity decreased slightly from 121 to 117, 111, and 104 mAh g^{-1}, respectively.

Fig. 12 shows cyclic voltammograms recorded at a scan rate of 0.07 mV s^{-1} of the pure and glass-modified $LiCoO_2$ powders post-treated at 600 °C. The peak positions of the glass-modified $LiCoO_2$ powders changed slightly more than those of the pure $LiCoO_2$ powders did. The surface compositions of the powders were determined by the XPS analysis. Fig. 13 shows the XPS spectra of the pure and 5 wt% glass-modified $LiCoO_2$ powders post-treated at 600 °C. Boron component was detected in the XPS spectrum of the 5 wt% glass-modified $LiCoO_2$ powders as shown by circle in Fig. 13. The binding energy of B 1s was 191.3 eV. The surface elemental composition of the 5 wt% glass-modified $LiCoO_2$ powders was $LiB_{1.05}Co_{0.45}O_{2.7}$. The coating layer formed on the surface, as well as the increased mean size, of the glass-modified $LiCoO_2$ powders improved the electrochemical properties of the powders by decreasing their reactivity with acidic electrolytes. The stabilization effect of B-doping in the $LiCoO_2$ powders also improved the electrochemical properties of the LBO glass-modified $LiCoO_2$ powders [36–38].

4. Conclusions

The electrochemical properties of LBO glass-modified $LiCoO_2$ nanopowders prepared by flame spray pyrolysis were investigated before and after post-treatment. The nanopowders demonstrated low initial charge/discharge capacities and poor cycle properties. However, $LiCoO_2$ powders modified with 5 wt% LBO glass had high initial charge/discharge capacities and good cycle properties after post-treatment at 600 and 700 °C. The mean sizes of the glass-modified $LiCoO_2$ powders were 92 and 120 nm after post-treatment at 600 and 700 °C, respectively. Therefore, the optimum post-treatment temperature for obtaining $LiCoO_2$ powders with nanometer-sized particles and good electrochemical properties was determined to be 600 °C. The coating layer formed on the surface and the increased mean size of the glass-modified $LiCoO_2$ particles improved the electrochemical properties of the powders by decreasing their reactivity with acidic electrolytes.

Acknowledgment

This work was supported by the National Research Foundation of Korea (NRF) grant funded by the Korea government (MEST) (No. 2012R1A2A2A02046367).

References

[1] M.S. Whittingham, Chem. Rev. 104 (2004) 4271.
[2] J.P. Cho, Y.J. Kim, B.W. Park, Chem. Mater. 12 (2000) 3788.
[3] Z.X. Wang, L.J. Liu, L.Q. Chen, X.J. Huang, Solid State Ionics 148 (2002) 335.
[4] X.L. Xiao, L.M. Yang, H. Zhao, Z.B. Hu, Y.D. Li, Nano Res. 5 (1) (2012) 27.
[5] Y.K. Sun, C.S. Yoon, S.T. Myung, I. Belharouak, K. Amine, J. Electrochem. Soc. 156 (12) (2009) A1005.
[6] Z. Chen, J.R. Dahn, Electrochim. Acta 49 (2004) 1079.
[7] N. Ohta, K. Takada, L. Zhang, R. Ma, M. Osada, T. Sasaki, Adv. Mater. 18 (2006) 2226.
[8] M.K. Jo, S.K. Jeong, J.P. Cho, Electrochem. Commun. 12 (2010) 992.
[9] M. Okubo, E. Hosono, J.D. Kim, M. Enomoto, N. Kojima, T. Kudo, H. Zhou, I. Honma, J. Am. Chem. Soc. 129 (2007) 7444.
[10] F. Jiao, K.M. Shaju, P.G. Bruce, Angew. Chem. Int. Ed. 44 (2005) 6550.
[11] Y. Gu, D. Chen, X. Jiao, J. Phys. Chem. B 109 (2005) 17901.
[12] Q. Wu, W. Li, Y. Cheng, Z. Jiang, Mater. Chem. Phys. 91 (2005) 463.
[13] M.K. Jo, Y.S. Hong, J.B. Choo, J.P. Cho, J. Elctrochem. Soc. 156 (6) (2009) A430.
[14] S.M. Lala, L.A. Montoro, J.M. Rosolen, J. Power Sources 124 (2003) 118.
[15] C.H. Han, Y.S. Hong, C.M. Park, K. Kim, J. Power Sources 92 (2001) 95.
[16] S.H. Ng, T.J. Patey, R. Büchel, F. Krumeich, J.Z. Wang, H.K. Liu, S.E. Pratsinis, P. Novák, Phys. Chem. Chem. Phys. 11 (2009) 3748.
[17] J.H. Kim, J.H. Yi, Y.N. Ko, Y.C. Kang, Mater. Chem. Phys. 134 (2012) 254.
[18] M. Yamada, B. Dongying, T. Kodera, K. Myoujin, T. Ogihara, J. Ceram. Soc. Jpn. 117 (2009) 1017.
[19] T.J. Patey, R. Buchel, S.H. Ng, F. Krumeich, S.E. Pratsinis, P. Novák, J. Power Sources 189 (2009) 149.
[20] T. Lee, K. Cho, J. Oh, D. Shin, J. Power Sources 174 (2007) 394.
[21] H.D. Jang, C.M. Seong, Y.J. Suh, H.C. Kim, C.K. Lee, Aerosol. Sci. Technol. 38 (2004) 1027.
[22] T.J. Patey, S.H. Ng, R. Buechel, N. Tran, F. Krumeich, J. Wang, H.K. Liu, P. Novák, Electrochem. Solid-State Lett. 11 (2008) A47.
[23] J.H. Yi, J.H. Kim, H.Y. Koo, Y.N. Ko, Y.C. Kang, J.H. Lee, J. Power Sources 196 (2011) 2858.
[24] P.G. Bruce, B. Scrosati, J.M. Tarascon, Angew. Chem. Int. Ed. 47 (2008) 2930.
[25] N.N. Sinha, N. Munichandraiah, J. Indian Inst. Sci. 89 (2009) 381.
[26] M. Okubo, E. Hosono, T. Kudo, H.S. Zhou, I. Honma, Solid State Ionics 180 (2009) 612.
[27] I.D. Scott, Y.S. Jung, A.S. Cavanagh, Y. Yan, A.C. Dillon, S.M. George, S.H. Lee, Nano Lett. 11 (2011) 414.
[28] Q. Hao, H. Ma, Z. Ju, G. Li, X. Li, L. Xu, Y. Qian, Electrochim. Acta 56 (2011) 9027.
[29] G.T.K. Fey, C.Z. Lu, T. Prem Kumar, Y.C. Chang, Surface Coat. Technol. 199 (2005) 22.
[30] Z.X. Wang, H. Dong, X.J. Huang, Y.J. Mo, L.Q. Chen, Electrochem. Solid-State Lett. 7 (2004) A353.
[31] G.G. Amatucci, J.M. Tarascon, Solid State Ionics 104 (1997) 13.
[32] H.W. Chan, J.G. Duh, S.R. Sheen, Surface Coat. Technol. 188 (2004) 116.
[33] H. Şahan, H. Göktepe, S. Patat, A. Ülgen, Solid State Ionics 178 (2008) 1837.
[34] J. Ying, C. Wan, C. Jiang, J. Power Sources 102 (2001) 162.
[35] S.H. Choi, J.H. Kim, Y.N. Ko, Y.J. Hong, Y.C. Kang, J. Power Sources 210 (2012) 110.
[36] A. Veluchamy, H. Ikuta, M. Wakihara, Solid State Ionics 143 (2001) 161.
[37] C.M. Julien, A. Mauger, H. Groult, X. Zhang, F. Gendron, Chem. Mater. 23 (2011) 208.
[38] C.M. Julien, Solid State Ionics 157 (2003) 57.